

Differential Geometry in Neural Implicits

Tiago Novello, Vinicius da Silva, Helio Lopes,
Guilherme Shardong, Luiz Schirmer, Luiz Velho

January 25, 2022

Abstract

We introduce a neural implicit framework that bridges discrete differential geometry of triangle meshes and continuous differential geometry of neural implicit surfaces. It exploits the differentiable properties of neural networks and the discrete geometry of triangle meshes to approximate them as the zero-level sets of *neural implicit functions*.

To train a neural implicit function, we propose a loss function that allows terms with high-order derivatives, such as the alignment between the principal directions, to learn more geometric details. During training, we consider a non-uniform sampling strategy based on the discrete curvatures of the triangle mesh to access points with more geometric details. This sampling implies faster learning while preserving geometric accuracy.

We present the analytical differential geometry formulas for neural surfaces, such as normal vectors and curvatures. We use them to render the surfaces using sphere tracing. Additionally, we propose a network optimization based on singular value decomposition to reduce the number of parameters.

1 Introduction

Level sets of neural networks have been used to represent implicit surfaces in \mathbb{R}^3 with accurate results. In this context, the *neural implicit problem* is the task of training the parameters θ of a neural network $f_\theta : \mathbb{R}^3 \rightarrow \mathbb{R}$ such that its *zero-level set* $f_\theta^{-1}(0) = \{p \mid f_\theta(p) = 0\}$ approximates a desired surface in \mathbb{R}^3 . We say that f_θ is a *neural implicit function* and that $f_\theta^{-1}(0)$ is a *neural implicit surface*.

This work explores the *differential geometry* of (implicit) surfaces in the learning process of the neural implicit function f_θ . For this, we need f_θ to be a smooth function (or at least C^2). *Sinusoidal representation networks* (SIREN) [48] and *implicit geometric representation* (IGR) [19] are examples of neural network architectures that provide smooth neural implicit functions. We adopt as a basis the SIREN architecture which has important properties that are suitable for reconstructing signals.

Specifically, let S be a surface in \mathbb{R}^3 , and $f_\theta : \mathbb{R}^3 \rightarrow \mathbb{R}$ be a neural implicit function with an *unknown* set of parameters θ . Given a sample of S , we look for a θ such that f_θ approximates the *signed distance function* of S . It is well-known that signed distance functions have unit gradient. Therefore, we ask f_θ to satisfy the *Eikonal equation* $|\nabla f_\theta| = 1$. Moreover, it is required the conditions $f_\theta = 0$ and $\langle \nabla f_\theta, N \rangle = 1$ on S , which force f_θ to be a signed distance function of S and its gradient to be aligned to the normals N of S . To use such constraints in a loss function, we need f_θ to be differentiable.

The above constraints require two degrees of differentiability of f_θ . This work will also explore the "alignments" between the *shape operator* $d\frac{\nabla f_\theta}{|\nabla f_\theta|}$ of the neural surface $f_\theta^{-1}(0)$ and the shape operator dN of S . This requires one more degree (C^3) of differentiability of f_θ . As the shape operators carry the intrinsic/extrinsic geometry of their surfaces, asking their alignment would require more consistency between the geometrical features of $f_\theta^{-1}(0)$ and S .

In practice, we have a sample of points of S . Suppose that the shape operator is known at these points. During the training of f_θ , it is common to sample batches of points uniformly. However, there is a high probability of selecting points with poor geometric details on their neighborhoods, which leads to slow learning of the network. This is probably a consequence of the *Gauss–Bonnet theorem* $\int_S K dS = 2\pi\chi(S)$, where K is the *Gaussian curvature*, and $\chi(S)$ is the *Euler characteristic* of S . This work proposes a sampling based on the curvature to select points with important geometric details during the training.

With a trained neural implicit function f_θ in hand, we can analytically calculate the differential geometry formulas of the corresponding neural implicit surface since we have its (neural) shape operator $d\frac{\nabla f_\theta}{|\nabla f_\theta|}$. We provide the formulas along with the text.

To visualize the neural surface $f_\theta^{-1}(0)$, we use the *sphere tracing algorithm* [21, 22] since f_θ is an approximation of a signed distance function. In this technique, f_θ is evaluated in a finite number of points along each view ray, then, it is desired to have the neural network f_θ optimized. For this, we apply *singular value decomposition* (SVD) in the hidden layers to reduce the number of parameters of the networks while it is maintained the main features.

The main contribution of our work is a global geometric representation in the continuous setting using neural networks as implicit functions. Besides its compact representation that captures geometrical details, this model is robust for shape analysis and efficient for computation since we have its derivatives in closed form. Specifically, we can summarize our contributions in four classes:

- A *loss functional* that allows the exploration of tools from continuous differential geometry during the training of the neural implicit function. This provides high fidelity when reconstructing geometric features of the surface.
- During the training of the neural implicit function, we use the discrete differential geometry of the dataset (triangle mesh) to *sample* important regions. This provides a robust and fast training without losing geometrical details.
- Defining the appropriate depth/width of the neural implicit function to represent a given surface remains an open problem. However, if the network has more capacity than is necessary, we propose an *optimization* of its parameters using SVD. This reduces the number of parameters allowing for efficient inference. When the network cannot represent a given surface, we increase the dimension of its hidden domains.
- To visualize neural implicit surfaces in real-time, we present an implementation of the (neural) sphere tracing in GPU. We also adopt the above network optimization for efficient memory usage during the sphere tracing.

In this work, we will focus on implicit surfaces in the three-dimensional Euclidean space \mathbb{R}^3 . However, the definitions and techniques that we are going to describe can be easily adapted to the context of implicit n -dimensional *manifolds* embedded in \mathbb{R}^{n+1} . In particular, it can be extended to curves and gray-scales images (graph of 2D functions). For neural surfaces animation, see [40].

2 Related concepts and previous works

The research topics related to our work include implicit surface representations using neural networks, discrete and continuous differential geometry, and surface reconstruction.

2.1 Surface representation

A regular surface S in \mathbb{R}^3 can be represented *explicitly* using a special collection (*atlas*) of *charts* that covers S or *implicitly* using an implicit function that has S as its zero-level set. The *implicit function theorem* defines a bridge between these two representations. Consider S to be a smooth surface, i.e. there is a smooth function $f : \mathbb{R}^3 \rightarrow \mathbb{R}$ having S as its zero-level set $f^{-1}(0)$ and $\nabla f \neq 0$ on it. The normalized gradient $N = \frac{\nabla f}{|\nabla f|}$ defines a *normal* field on S . The differential of N is an important object in differential geometry, it is a symmetric 2D tensor field over the surface, the *shape operator*. The eigenvalues and eigenvectors of this tensor are the *principal curvatures* and its *principal directions*. They indicate the directions in which the surface is most curved and least curved. In particular, they are tangent to perpendicular curves in S that can be used to create *anisotropic meshes* [30, 1].

In practice, we usually have a point cloud $\{p_i\}$ collected from a *real-world* surface S . It is common to consider an additional *triangle mesh* $T = (V, E, F)$, where $V = \{p_i\}$ are the vertices, E are the edges, and F are the triangles. T is a piecewise linear approximation of S with topological guarantees if it satisfies a set of special properties [2].

2.1.1 Discrete differential geometry

Unfortunately, the triangle mesh T is a piecewise linear approximation of the surface S . Therefore, its geometry cannot be studied in the classical differentiable way, since it does not admit a continuous normal field. However, we can define a *discrete* notion of this field. In this case, it is constant on each triangle and can be computed using the cross product. This implies a discontinuity of the field on the edges and vertices. To overcome this, we use an average of the normals of the adjacent faces [35]. In other words, the variations of the normal field are concentrated on the edges and vertices of T .

The study of the discrete variations of the normals of triangle meshes is an important topic in *discrete* differential geometry [35, 9, 50]. Again, these variations are encoded in a *discrete shape operator*. Specifically, the principal directions and curvatures can be defined on the edges. One of the curvatures is zero, along the edge direction, and the other one is measured across the edge and it is given by the dihedral angle between the adjacent faces. Finally, we can estimate the shape operator at the vertices by considering the average of the shape operator of the neighboring edges. We consider the approach of [9], which provides a reliable approximation if the triangle mesh satisfies a set of special properties.

There are several approaches to extend differential operators to triangle meshes. They all try to create discrete operators that mimic a certain set of natural properties inherent in the continuous setting. Most often, it is not possible to discretize a smooth object such that all of the natural properties are preserved — this is the *no free lunch* scenario. For instance, [52] proved that the existent discrete *Laplacians* do not satisfy the properties of the continuous Laplacian. For more details, see [10].

The curvature tensor of a (discrete) surface is an important measure and provides several applications such as surface reconstruction [18], surface segmentation [27], remeshing [1, 30], denoising [26], partial symmetry detection [38], feature line extraction [23], direct volume rendering [24], image synthesis [45], among others.

In this work, we propose to use the shape operator in a implicit surface representation using neural networks. In this setting, a neural network is used to model an unknown smooth implicit function. The parameters of the resulting *neural implicit function* are trained using a dataset that we are considering to be a triangle mesh, however, it could be a more general polygonal mesh or a point cloud. The only requirement is to have a discrete curvature tensor associated with the dataset. A loss function is designed to fit the zero-level set of the neural implicit function to the dataset. We propose to use the discrete shape operator in the loss function to enforce the learning of more geometrical detail, and during the sampling to consider minibatches biased by the discrete curvature of the data.

2.2 Neural implicit representations

In the context of implicit surface representations using neural networks, we can divide the methods in three categories: 1st generation models; 2nd generation models; 3rd generation models.

The first generation models correspond to *global* functions of the ambient space and employ as implicit model either a *characteristic function* or a *generalized signed distance function*. They use a fully connected multi layer perceptron network architecture. The model is learned by fitting the input data to the model. The loss function is based either on the L_1 or L_2 norm. The seminal papers of this category appeared in 2019. They are: Occupancy Networks [34], Learned Implicit Fields [8], Deep SDF [43], and Deep Level Sets [36].

The second generation models correspond to a set of *local* functions that combined together gives a representation of a function over the whole space. These models are based either on a shape algebra, such as in *constructive solid geometry*, or convolutional operators. The seminal papers of this category appeared in 2019 / 2020. They are: Local Deep Implicit Functions [16], BSP-Net [7], CvxNet [14] and Convolutional Occupancy Networks [44].

The third generation models correspond to true signed distance functions that are given by the *Eikonal* equation. The model exploits in the loss function the condition that the gradient of the function has unitary norm everywhere, i.e., $|\nabla f| = 1$. The seminal papers of this category appeared in 2020. They are: IGR [19] and SIREN [48].

Inspired by the third generation models, we explore smooth neural networks that can represent the signed distance functions of surfaces. That is, the Eikonal equation will be considered in the loss function which add constraints involving derivatives of first order of the underlying function. Moreover, we consider higher order derivatives of the network, by proposing the use of differential geometry tools

in the loss function, during its training and sampling, and on its optimization. The smooth network utilized in the framework is a multi layer perceptron with a smooth activation function.

The neural implicit problem is related to the *regression* problem since it consists of finding the parameters of a network such that it fits to the signed distance of a given surface. Therefore, the neural implicit problem is close to the problem of reconstructing a surface.

2.3 Radial basis functions

Radial basis functions [6] is a classical technique to reconstruct an implicit function $f : \mathbb{R}^3 \rightarrow \mathbb{R}$ from a point cloud $\{p_i\}_{i=1}^n$ using the smooth interpolation: $s(p) = g(p) + \sum \lambda_i \phi(|p - p_i|)$, where g is a low degree polynomial, λ_i are real numbers, the *basic function* $\phi : \mathbb{R}^+ \rightarrow \mathbb{R}^+$ is a real function, and p_i are the centers of the radial basis function. Common choices of the basic function include $\phi(r) = r$ and $\phi(r) = r^3$. In case the dataset is endowed with normals $\{p_i, N_i\}_{i=1}^n$, [29] proposed to approximate the function f by a *Hermite* radial basis function.

It is important to note that the representation of the radial basis function s is directly dependent on the size n of the dataset.

Our neural implicit framework supports flexible implicit reconstruction with high fidelity and allows a compact representation of the implicit functions.

2.4 Continuous volumetric functions

Alternatively to implicit surface descriptions it is possible to model continuous volumetric functions that encode *radiance fields*. They represent geometry as a density over space and also encode direction-dependent radiance information. The seminal papers of this category appeared in 2020 /2021. They are: NeRF [37], MNSR [54], among many others.

Recently, there is a trend to combine Neural Implicit Representations with Neural Volumetric Radiance Fields. The main papers in this regard are: UNISURF [41], NeuS [51], and VolSDF [53].

2.5 Visualizing neural implicit surfaces

The initial works in neural implicit representation use marching cubes [28] to generate visualizations of the resulting (neural) level sets. This approach is probably a consequence of visualization not being the major focus of those works and of the usual development environment for learning algorithms. Marching cubes has a few dramatic drawbacks in this context: it is very sensitive to grid discretization and it is not interactive. Without a high resolution grid, marching cubes can lose high frequencies on reconstruction. The need for high resolution also demands processing, making its performance prohibitive for real-time applications.

Subsequent works propose spatial hierarchies of small neural networks [49, 31]. Although this is the state-of-art in terms of neural implicit rendering performance, it comes with essential changes to training and workflow.

We visualize neural implicit surfaces using sphere tracing. It is already possible to make neural implicit inferences on rendering [13], but the capacity of these networks does not seem to represent high frequencies. We propose to combine sphere tracing with an optimization of our neural implicit architecture to render images of neural implicit surface in real-time.

3 Conceptualization

3.1 Implicit surfaces

The zero-level set $f^{-1}(0)$ of an *implicit function* $f : \mathbb{R}^3 \rightarrow \mathbb{R}$ can be used to represent a surface S in \mathbb{R}^3 . If f is smooth and has $c \in \mathbb{R}$ as a regular value, then its c -level set is a regular surface S . A number $c \in f(\mathbb{R}^3)$ is a *regular value* of f iff $\nabla f \neq 0$ in $f^{-1}(c)$. Conversely, let S be a regular surface in \mathbb{R}^3 , there is a function $f : \mathbb{R}^3 \rightarrow \mathbb{R}$ having S as its c -level set, i.e. $f^{-1}(c) = S$ [15, Page 116]. Therefore, given a sample of points on the surface S , we could try to construct the corresponding implicit function f .

3.1.1 Differential geometry of implicit surfaces

Let S be a regular surface and $f : \mathbb{R}^3 \rightarrow \mathbb{R}$ be its implicit function. The differential $dN_p : T_p S \rightarrow T_p S$ of $N = \frac{\nabla f}{|\nabla f|}$ at $p \in S$ is a linear map on the tangent plane $T_p S$. The map dN is called the *shape operator* of S and can be expressed by the following formula:

$$dN = (I - N \cdot N^\top) \frac{\mathbf{H}f}{|\nabla f|}, \quad (1)$$

where $\mathbf{H}f$ denotes the *Hessian* of f and I is the identity matrix. Thus, the shape operator is the product of the Hessian (scaled by the gradient norm) and a linear projection along the normal N .

As dN_p is symmetric, the spectral theorem states that there is an orthogonal basis $\{e_1, e_2\}$ of $T_p S$ (the *principal directions*) where dN_p can be expressed as a diagonal 2×2 matrix. The two elements of this diagonal are the *principal curvatures* κ_1 and κ_2 , and are obtained using $dN(e_i) = -\kappa_i e_i$.

The *second fundamental form* of S can be used to interpret dN geometrically. It is a map that attributes to each point $p \in S$ the quadratic form $\mathbf{II}_p(v) = \langle -dN_p(v), v \rangle$ on $T_p S$. Let α be a curve passing through p with unit tangent direction v . The number $\kappa_n(p) = \mathbf{II}_p(v)$ is the *normal curvature* of α at p . [24] used κ_n to control the width of the *silhouettes* of S at rendering.

Restricted to the unit circle of $T_p S$, \mathbf{II}_p reaches a maximum and a minimum (principal curvatures). In the frame $\{e_1, e_2\}$, \mathbf{II}_p can be written in the quadratic form $\mathbf{II}_p(v) = x_1^2 \kappa_1 + x_2^2 \kappa_2$ with $v = x_1 e_1 + x_2 e_2$. Points can be classified based on their form: *elliptic* if $\kappa_1 \kappa_2 > 0$, *hyperbolic* if $\kappa_1 \kappa_2 < 0$, *parabolic* if only one κ_i is zero, and *planar* if $\kappa_1 = \kappa_2 = 0$. This classification is related to the *Gaussian curvature* $K = \kappa_1 \kappa_2$. Elliptic points have positive curvature. At these points, the surface is similar to a dome, positioning itself on one side of its tangent plane. Hyperbolic points have negative curvature. At such points, the surface is saddle-shaped. Parabolic and planar points have zero curvature.

The Gaussian curvature K of the surface S can be calculated using the following formula [17].

$$K = -\frac{1}{|\nabla f|^4} \det \left[\begin{array}{c|c} \mathbf{H}f & \nabla f \\ \hline \nabla f^\top & 0 \end{array} \right]. \quad (2)$$

The *mean curvature* $H = (\kappa_1 + \kappa_2)/2$, is an extrinsic measure that describes the curvature of the embedded surface S in \mathbb{R}^3 . It is the half of the *trace* of dN which does not depend on the choice of basis. Expanding it results in the divergence of N , implying in the simple formula $2H = \operatorname{div} \frac{\nabla f}{|\nabla f|}$. Thus, if f is a signed distance function, the mean curvature can be written using the Laplacian Δf .

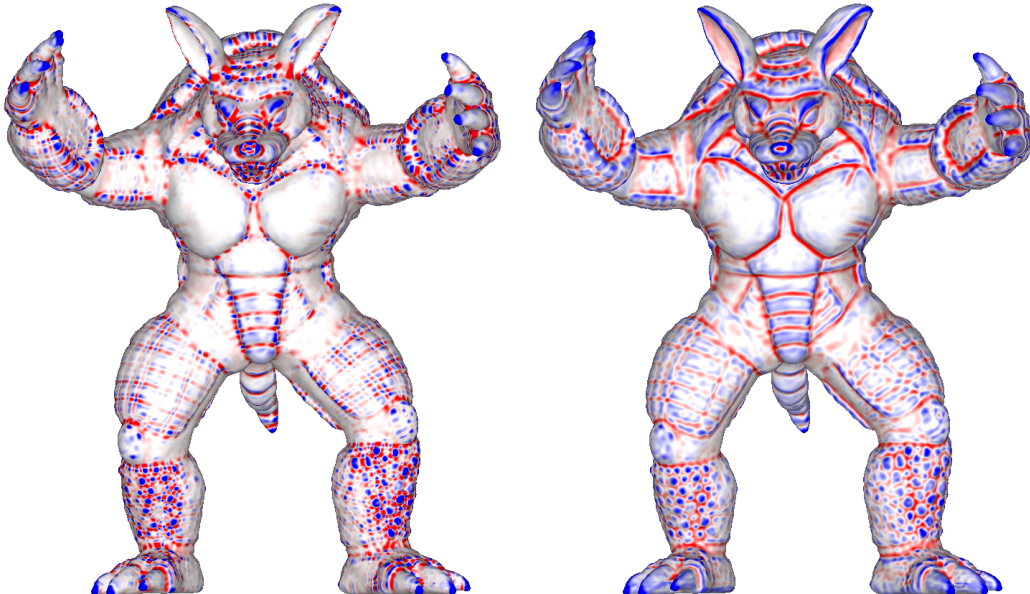


Figure 1: Gaussian and mean curvatures of the smooth Armadillo model.

An important advantage of representing a surface using level sets of implicit functions is that the geometric objects, like normals and curvatures, can be computed analytically — no discretization is need. Figure 1 illustrates the Gaussian and mean curvature of a smooth implicit surface approximating the Armadillo model. The implicit function was computed using the framework we are proposing.

There are several representations of implicit functions. For example, in *constructive solid geometry* the object is represented by combining simple objects (primitives) using union, intersection, and difference. However, this approach has limitations. For instance, representing a complex geometry such as the Armadillo would require a prohibitive number of operations. Another successful approach is using radial basis functions. However, it is not a compact representation since it depends on the size of the data set. A neural network is an option that can represent any function, which is guaranteed by the *universal approximation theorem*.

3.2 Neural implicit surfaces

A *neural implicit function* $f_\theta : \mathbb{R}^3 \rightarrow \mathbb{R}$ is an implicit function modeled by a neural network. We call the zero-level set $f_\theta^{-1}(0)$ a *neural implicit surface*. Let S be a compact surface in \mathbb{R}^3 , and $f_\theta : \mathbb{R}^3 \rightarrow \mathbb{R}$ be an unknown neural implicit function. To compute the parameter set of f_θ such that $f_\theta^{-1}(0)$ approximates S , it is common to consider the following *Eikonal* problem in the loss function.

$$\begin{cases} |\nabla f_\theta| = 1 & \text{in } \mathbb{R}^3, \\ f_\theta = 0 & \text{on } S, \\ \frac{\partial f_\theta}{\partial N} = 1 & \text{on } S \end{cases} \quad (3)$$

The *Eikonal equation* $|\nabla f_\theta| = 1$ asks for f_θ to be a *signed distance function*. The *Dirichlet condition*, $f_\theta = 0$ on S , requires f_θ to be the signed distance from a set that contains S . The *Neumann condition*, $\frac{\partial f_\theta}{\partial N} = 1$ on S , forces ∇f_θ to be aligned to the normal field N of S . This is due to the fact that $\frac{\partial f_\theta}{\partial N} = \langle \nabla f_\theta, N \rangle$. Observe that these constraints requires two degree of differentiability of f_θ . Therefore, we will restrict our study to smooth neural implicit functions.

There are several advantages of using neural surfaces. Besides having the entire framework of neural networks available, neural functions have a high capacity of representation due to the approximation theorems. We also have access to the differential geometry tools of neural surfaces, for this, we only need the Hessian and gradient operators of the network since these are ingredients for the shape operator (Eq. 1). As a consequence, we can design loss functions using high-order differential terms computed analytically.

3.3 Learning a neural implicit surface

Let S be a compact surface in \mathbb{R}^3 and $f : \mathbb{R}^3 \rightarrow \mathbb{R}$ be its signed distance function. Let $f_\theta : \mathbb{R}^3 \rightarrow \mathbb{R}$ be an *unknown* neural implicit function. To train its parameters θ , we seek a minimum of the following loss function, which forces f_θ to be a solution of Equation (3).

$$\mathcal{L}(\theta) = \underbrace{\int_{\mathbb{R}^3} |1 - |\nabla f_\theta|| dp}_{\mathcal{L}_{\text{Eikonal}}} + \underbrace{\int_S |f_\theta| dS}_{\mathcal{L}_{\text{Dirichlet}}} + \underbrace{\int_S 1 - \langle \nabla f_\theta, N \rangle dS}_{\mathcal{L}_{\text{Neumann}}}. \quad (4)$$

$\mathcal{L}_{\text{Eikonal}}$ encourages f_θ to be the signed distance of a set $\mathcal{X} \subset \mathbb{R}^3$ by forcing it to be a solution of $|\nabla f_\theta| = 1$. $\mathcal{L}_{\text{Dirichlet}}$ encourages \mathcal{X} to contain the surface S . $\mathcal{L}_{\text{Neumann}}$ asks for the gradient ∇f_θ and the normal field of S to be aligned. It is common to consider an additional term in Equation (4) penalizing off point of S , this forces f_θ to be a signed distance function from S .

We investigate the use of the shape operator dN of $f_\theta^{-1}(0)$ to improve \mathcal{L} , by forcing dN to align with the *discrete* shape operator of the ground truth triangle mesh. For the sampling of points used to feed a discretization of \mathcal{L} , we consider the corresponding discrete curvatures to access regions containing appropriate features.

3.4 Discrete surfaces

Let $T = (V, E, F)$ be a triangle mesh representing a piecewise linear approximation of S . $V = \{p_i\}$ are the vertices, E denotes the edge set, and T denotes the triangle set. The discrete curvature measures of T are concentrated on its vertices and can be computed using its *discrete shape operator* [9].

$$\mathcal{S}(p_i) = \frac{1}{|B|} \sum_{e \in E} \beta(e) |e \cap B| \bar{e} \cdot \bar{e}^\top. \quad (5)$$

Where $p_i \in V$, $|B|$ is the area of a neighborhood B of p_i , $\beta(e)$ is the signed dihedral angle between the two faces adjacent to e , $|e \cap B|$ is the length of $e \cap B$, and \bar{e} is a unit vector aligned to e . Figure 2 shows a schematic illustration of the discrete shape operator. It is common to consider B being the dual face of the vertex. The discrete shape operator is the discrete analogous to the shape operator (Eq. (1)).

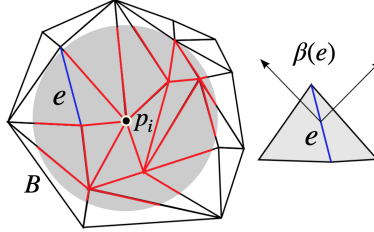


Figure 2: Discrete shape operator setting.

As in the continuous case, the discrete shape operator is a 3×3 matrix, and in this case it is symmetric. Then, there are exactly three eigenvalues and their respective eigenvectors. The normal N_i is the eigenvector associated with the smaller (in absolute) eigenvalue. The remaining eigenvalues are the principal discrete curvatures, and their associated eigenvectors are the principal discrete directions. The principal curvatures and principal directions are permuted. The *discrete Gaussian curvature* K_i and *mean curvature* H_i at a vertex p_i are the product and the average of the principal discrete curvatures.

4 Differentiable Neural Implicits

This section explores the differential geometry of the zero-level sets of smooth neural implicit functions during their training. For the sampling, we use the discrete differential geometry of the dataset triangle mesh to prioritize important features. Finally, we propose an optimization of the parameters of the network, which we use to visualize the surface in real-time.

4.1 Neural implicit function architecture

We consider the neural implicit function $f_\theta : \mathbb{R}^3 \rightarrow \mathbb{R}$ defined by

$$f_\theta(p) = W_n \circ f_{n-1} \circ f_{n-2} \circ \cdots \circ f_0(p) + b_n \quad (6)$$

where $f_i(p_i) = \varphi(W_i p_i + b_i)$ is the i th layer obtained by applying a smooth *activation function* $\varphi : \mathbb{R} \rightarrow \mathbb{R}$ to each coordinate of the affine map given by the linear transformation $W_i : \mathbb{R}^{N_i} \rightarrow \mathbb{R}^{N_{i+1}}$ translated by the *bias* $b_i \in \mathbb{R}^{N_{i+1}}$. The linear operators W_i can be represented as matrices and b_i as vectors. Therefore, the union of their coefficients corresponds to the parameters θ of f_θ .

We consider φ to be the sine function since the resulting network is suitable for reconstructing signals and can approximate all continuous functions in the cube $[-1, 1]^3$ [11]. Recently, [48] proposed an initialization scheme for training the parameters of the network in the general context of signal reconstruction — implicit surfaces being a particular case. Here, we explore the main properties of this definition in implicit surface reconstruction. For example, its first layer is related to a *Fourier feature mapping* [5], which allows us to represent high-frequency three-dimensional implicit functions.

Another property of this network is its smoothness, which enables the use of differential geometry in the framework. For example, by Equation 1, the *neural shape operator* of a neural surface can be computed using only its gradient and Hessian operators, which we are going to present in closed form in the next sections. These operators are also helpful during training and shading.

We are using the multilayer perceptron network architecture defined in Equation 6, however, any smooth neural function could be adapted to our framework.

4.1.1 Gradient of a neural implicit function

The neural implicit function f_θ is smooth since its partial derivatives (of all orders) exist and are continuous. Indeed, each function f_i has all the partial derivatives because, by definition, it is an affine map with the smooth activation function φ applied to each coordinate. Therefore, the chain rule implies the smoothness of f_θ . We can compute the gradient of f_θ explicitly:

$$\nabla f_\theta(p) = \mathbf{J}(W_n \circ f_{n-1} \circ \cdots \circ f_0(p)) + \mathbf{J}(b_n) = \mathbf{J}W_n(f_{n-1} \circ \cdots \circ f_0(p)) \cdot \cdots \cdot \mathbf{J}f_1(f_0(p)) \cdot \mathbf{J}f_0(p),$$

where \mathbf{J} is the *Jacobian*. Using that $\mathbf{J}(b_n) = 0$ and $\mathbf{J}W_n(q) = W_n$, because W_n is linear, we obtain:

$$\nabla f_\theta(p) = W_n \cdot \mathbf{J}f_{n-1}(p_{n-1}) \cdot \cdots \cdot \mathbf{J}f_1(p_1) \cdot \mathbf{J}f_0(p), \quad (7)$$

with $p_i = f_{i-1} \circ \cdots \circ f_0(p)$. Calculations lead us to an explicit formula for the Jacobian of f_i at p_i .

$$\mathbf{J}f_i(p_i) = W_i \odot \varphi' [a_i | \cdots | a_i] \quad (8)$$

where \odot is the *Hadamard* product, and the matrix $[a_i | \cdots | a_i]$ has N_i copies of $a_i = W_i(p_i) + b_i \in \mathbb{R}^{N_{i+1}}$.

4.1.2 Hessian of a neural implicit function

Recall the *chain rule* formula for the *Hessian* operator of the composition of two maps $f : \mathbb{R}^m \rightarrow \mathbb{R}^n$ and $g : \mathbb{R}^n \rightarrow \mathbb{R}$:

$$\mathbf{H}(g \circ f)(p) = \mathbf{J}f(p)^\top \cdot \mathbf{H}g(f(p)) \cdot \mathbf{J}f(p) + \mathbf{J}g(f(p)) \cdot \mathbf{H}f(p) \quad (9)$$

We consider this formula to compute the hessian $\mathbf{H}f_\theta$ of the neural implicit function f_θ using induction on the layers of the network.

Let $f = f_{i-1} \circ \cdots \circ f_0$ be the composition of the first i layers of f_θ , and g be the l -coordinate of the i -layer f_i . Suppose we have the hessian $\mathbf{H}f(p)$ and jacobian $\mathbf{J}f(p)$ of f , from the previous steps of the induction. Then we only have to compute the hessian $\mathbf{H}g(f(p))$ and jacobian $\mathbf{J}g(f(p))$ of g in order to obtain $\mathbf{H}(g \circ f)(p)$. The formula for the jacobian of a hidden layer is presented in Equation (8).

Expanding the Hessian $\mathbf{H}g(p)$ of the layer $g(p) = \varphi(w_l p + b_l)$ gives us the following formula

$$\mathbf{H}g(p) = w_l^\top w_l \cdot \varphi''(w_l p + b_l). \quad (10)$$

Where w_l is the l th line of W and b_l is the l th coordinate of the bias b . Note that when using $\varphi = \sin$, we have $\mathbf{H}g(p) = -w_l^\top w_l \cdot g(p)$.

4.2 Loss functional

Let S be a compact surface in \mathbb{R}^3 and $f : \mathbb{R}^3 \rightarrow \mathbb{R}$ be its signed distance function. In this section, we explore the loss functional $\mathcal{L} = \mathcal{L}_{\text{Eikonal}} + \mathcal{L}_{\text{Dirichlet}} + \mathcal{L}_{\text{Neumann}}$ used to train a neural implicit function $f_\theta : \mathbb{R}^3 \rightarrow \mathbb{R}$ to approximate f . The training consists of seeking a global minimum θ of \mathcal{L} using the *gradient descent*. Here, we present ways of improving the Dirichlet and Neumann constraints.

4.2.1 Signed distance constraint

In practice we have a point cloud $\{p_i\}_{i=1}^n$ sampled from the surface S . We consider $\{p_i\}_{i=1}^n$ to be the set of vertices of a triangulation T of S . Then we replace $\mathcal{L}_{\text{Dirichlet}}$ by

$$\tilde{\mathcal{L}}_{\text{Dirichlet}}(\theta) = \frac{1}{n} \sum_{i=1}^n |f_\theta(p_i)|. \quad (11)$$

This constraint forces $f_\theta = f$ on $\{p_i\}_{i=1}^n$, which is equivalent to asking for $\{p_i\} \subset f_\theta^{-1}(0)$. However, the neural implicit surface $f_\theta^{-1}(0)$ could contain undesired spurious components. To avoid this, we extended the domain of $\tilde{\mathcal{L}}_{\text{Dirichlet}}$ in order to include off-surface points. For this, consider the point

cloud $\{p_i\}_{i=1}^{n+k}$ to be the union of the n vertices of T and a sample of k off-surface points in $\mathbb{R}^3 - S$. Then the Dirichlet constraint can be extended as follows.

$$\tilde{\mathcal{L}}_{\text{Dirichlet}}(\theta) = \frac{1}{n+k} \sum_{i=1}^{n+k} |f_\theta(p_i) - f(p_i)| \quad (12)$$

To compute an approximation of f in the off-surface point $\{p_i\}_{i=n+1}^{n+k}$, we use the algorithm presented in Section 4.2.2.

[48] uses an additional constraint $\int e^{-\alpha|f_\theta|} dp$, $\alpha > 1$, to penalize off-surface points. However, this constraint takes a while to remove the spurious components in $f_\theta^{-1}(0)$, it also adds some undesired smoothness to $f_\theta^{-1}(0)$. [19] uses a pre-training with off-surface points. Here, we use an approximation of the signed distance function during the sampling. This strategy is part of our framework using computational/differential geometry.

4.2.2 Signed distance function

Here we describe an approximation of the signed distance function $f : \mathbb{R}^3 \rightarrow \mathbb{R}$ of the compact surface S for use during the training of the neural implicit function f_θ . For this, we simply use the vertices $\{p_i\}_{i=1}^n$ of the triangle mesh T to approximate the absolute of the signed distance function f :

$$|f(p)| \approx \min_{i \leq n} |p - p_i| \quad (13)$$

The sign of f is approximated by checking if p is inside T . For this, we consider a spatial-indexing structure, such as Octrees or KD-trees, to store the triangle mesh T .

The sign of $f(p)$ at a point p is negative if p is inside T and positive otherwise. Observe that for each vertex p_i with a normal vector N_i , the sign of $\langle p - p_i, N_i \rangle$ indicates the side of the tangent plane that p belongs. Therefore, we approximate the sign of $f(p)$ by adopting the dominant signs of the numbers $\langle p - p_j, N_j \rangle$, where $\{p_j\} \subset V$ is a set of vertices close to p . This set can be estimated using the data structure.

4.2.3 Loss function using curvatures

The on-surface constraint $\int 1 - \langle \nabla f_\theta, N \rangle dS$ requires the gradient of the neural implicit function f_θ to be aligned to the normals of S . We extend this constraint by asking for the matching between the shape operator of the implicit surface $f_\theta^{-1}(0)$ and the shape operator of S . This can be done by requiring the alignment between their eigenvectors and the matching of their eigenvalues. Minimizing the following term results in the desired optimization.

$$\int_S \sum_{i=1,2,3} \left(1 - \langle (e_i)_\theta, e_i \rangle + |(\kappa_i)_\theta - \kappa_i| \right) dS \quad (14)$$

where $(e_i)_\theta$ and $(\kappa_i)_\theta$ are the eigenvectors and eigenvalues of the shape operator of $f_\theta^{-1}(0)$, and e_i and κ_i are the eigenvectors and eigenvalues of the shape operator of S . As the normal is, for both surfaces $f_\theta^{-1}(0)$ and S , one of the shape operator eigenvectors associated to the zero eigenvalue, Equation (14) is equivalent to:

$$\int_S 1 - \langle \nabla f_\theta, N \rangle dS + \int_S \sum_{i=1,2} \left(1 - \langle (e_i)_\theta, e_i \rangle + |(\kappa_i)_\theta - \kappa_i| \right) dS \quad (15)$$

The first integral in Equation (15) coincides with $\mathcal{L}_{\text{Neumann}}$. In the second integral, the term $1 - \langle (e_i)_\theta, e_i \rangle$ requires the alignment between the principal directions, and $|(\kappa_i)_\theta - \kappa_i|$ asks for the matching of the principal curvatures. Observe that asking for the alignment between $(e_1)_\theta$ and e_1 already forces the alignment between $(e_2)_\theta$ and e_2 , since the principal directions are orthogonal.

We can weaken the second integral of Equation (15) by considering the difference between the mean curvatures $|H_\theta - H|$ instead of $|(\kappa_1)_\theta - \kappa_1| + |(\kappa_2)_\theta - \kappa_2|$. This is a weaker restriction because $|H_\theta - H| \leq \frac{1}{2}|(\kappa_1)_\theta - \kappa_1| + \frac{1}{2}|(\kappa_2)_\theta - \kappa_2|$. However, it reduces the computations during optimization, since the mean curvature H_θ is calculated through the divergence of $\frac{\nabla f_\theta}{|\nabla f_\theta|}$.

Next, we present the sampling strategies mentioned above for use in the training process of the neural implicit function f_θ .

4.3 Sampling

Let $T = (V, E, F)$ be a triangle mesh approximating an *unknown* compact surface S in \mathbb{R}^3 . We assume that the n vertices $V = \{p_i\}$ of T are contained in S . Let $f_\theta : \mathbb{R}^3 \rightarrow \mathbb{R}$ be a neural implicit function with an unknown set of parameters θ . As we saw in Section 4.2, the training of θ consists of using the loss function \mathcal{L} to force f_θ to be the signed distance of S . In particular, it asks $f_\theta = 0$ in $\{p_i\}$.

In practice, the loss function \mathcal{L} is evaluated on a dataset of points dynamically sampled at training time. This dataset consists of a sampling of on-surface points in the vertices $\{p_i\}$ of T and a sampling of off-surface points in $\mathbb{R}^3 - S$. For the off-surface points, we opted for an uniform sampling in the domain of f_θ , however, in Section 6.1 we present a possible path for future work using the tubular neighborhood of T .

The loss functional \mathcal{L} requires on-surface samples of the form $\{p_i, N_i, \mathcal{S}_i\}$, where $\{p_i\}$ are vertices in T , $\{N_i\}$ are their normals $\{N_i\}$, and $\{\mathcal{S}_i\}$ are the discrete shape operators evaluated on the vertices. The normal N_i is defined by the average of the normal vectors of the faces adjacent to the vertex p_i . The discrete shape operator \mathcal{S}_i at p_i can be computed using Equation (5).

The discrete shape operator \mathcal{S} encodes important geometric features of the triangle mesh T . For example, regions containing vertices with higher principal curvatures κ_1 and κ_2 (eigenvalues of \mathcal{S}) in absolute codify more details than points with lower absolute curvatures. These are the elliptic ($\kappa_1\kappa_2 > 0$), hyperbolic ($\kappa_1\kappa_2 < 0$), or parabolic points (when only one κ_i is zero). Regions consisting of points close to planar, where $|\kappa_1|$ and $|\kappa_2|$ are close to zero, contain less geometric information, therefore, we do not need to visit all of them during each sampling. Also, planar points are, in general, abundant, for example, see Figure 1.

Based on the above discussion, we propose a non-uniform strategy to select the on-surface samples $\{p_i\}$ using their curvatures to obtain faster learning but the same quality. Specifically, we divide the vertices $\{p_i\}$ of T in three sets V_1, V_2 , and V_3 with *low*, *medium*, and *high* feature points. We use a *feature* function defined by the sum of the absolute of the principal curvatures $\kappa(p_i) = |\kappa_1(p_i)| + |\kappa_2(p_i)|$. Then, choosing $n = n_1 + n_2 + n_3$, with $n_i > 0$ integer, and sorting $\{p_i\}$ using κ , we define $V_1 = \{p_i | i \leq n_1\}$, $V_2 = \{p_i | i > n_1 \text{ and } i \leq n_2\}$, and $V_3 = \{p_i | i > n_2\}$. Therefore, the low feature points are related to the planar points, and the medium and high feature points are related to the parabolic, hyperbolic and parabolic points.

Therefore, during the training of the neural implicit function f_θ , we can prioritize points with more geometrical features, those in $V_2 \cup V_3$, to accelerate the learning. For this, we sample less low feature points in V_1 , which contains data redundancy, and increase the sampling in V_2 and V_3 .

We chose the partition $V_1 \cup V_2 \cup V_3$ because it showed good results, see the experiments in Section 5.2. However, it is one of the possible partitions. In future works, we intend to use the regions contained in the neighborhood of extremes of the principal curvatures, the so-called *ridges* and *ravines*. Section 5.2 presents more details.

4.4 Network optimization

The universal approximation theorems say that a neural network with arbitrary width and depth can approximate every implicit function. However, estimating the minimum network that represents a surface remains an open problem. In practice, we consider a network with fixed depth and width (found empirically), so that it can represent a given class of surfaces. Then, for a fixed surface, the network has a large representation capacity. Therefore, we can optimize the network parameters to get a compact representation.

Inspired by Faster-RCNN [46], we propose a network optimization that factorizes the hidden weight matrices using Singular Value Decomposition (SVD). Remember that the SVD of a matrix $W_{n \times m}$ uses the eigenvalues and eigenvectors of the symmetric, positive semidefinite matrices WW^\top and $W^\top W$. These two squared matrices have same rank r of W . The SVD theorem says that $W_{n \times m} = U_{n \times r} S_{r \times r} V_{m \times r}^\top$, where the r eigenvectors of WW^\top make up the columns of U and the r eigenvectors of $W^\top W$, the lines of V . The matrix S is diagonal and contains the square root of the non-zero eigenvalues of WW^\top (and $W^\top W$) in descending order.

We approximate the r -rank matrix W by a $(r-s)$ -rank matrix W_{r-s} by setting the s smallest singular values to zero. This reduces the dimension r of $U_{n \times r}, S_{r \times r}, V_{m \times r}^\top$, since it eliminates the s corresponding columns of U and V^\top . The resulting matrix W_{r-s} is the closest $(r-s)$ -rank matrix to W . This is a consequence of the Eckart-Young theorem: if B has rank $r-s$ then $|W - W_{r-s}| \leq |W - B|$.

It is well known that computing the SVD of a matrix $W_{n \times m}$ may be expensive since its complexity is $O(mn^2)$. We explore a computationally efficient way to compute a r -rank approximation of W , the *randomized SVD* [32]. This technique has two major steps. First, we multiply W by a Gaussian random matrix $\Omega_{n \times (r+k)}$, where $k > 0$ and $r+k \leq \min\{m, n\}$, to obtain a random linear combination of the columns of W . Next, a QR factorization of $W\Omega$ is used to provide an approximation of W given by $QQ^\top W$. The second step computes the SVD of the smaller matrix $Q^\top W = \hat{U}S\hat{V}^\top$. Truncating this decomposition to the desired rank r , and defining $U = Q\hat{U}$, we get the final approximation $W \approx QQ^\top W = USV^\top$. Algorithm 1 encodes the above procedure which has a computational cost of $2(r+k)O(\text{NonZeros}(W)) + O(r^2(m+n))$.

ALGORITHM 1: Randomized SVD

Input: matrix $W \in \mathbb{R}^{m \times n}$, rank r , oversampling parameter k
Output: matrices $U \in \mathbb{R}^{m \times r}, S \in \mathbb{R}^{r \times r}, V \in \mathbb{R}^{n \times r}$
Generate Gaussian random matrix $\Omega \in \mathbb{R}^{n \times (r+k)}$;
 $Y \leftarrow W\Omega$;
Compute the QR factorization of Y ;
 $B \leftarrow Q^\top W$;
Calculate the SVD $\hat{U}S\hat{V}^\top$ of B ;
 $U \leftarrow Q\hat{U}[:, 1:r]$;
return $U, S[1:r, 1:r], V[:, 1:r]$;

A fully connected layer $Wp + b$ does matrix multiplication of its input p by a matrix W , and then adds a bias b . Algorithm 1 approximates W by a r -rank matrix USV^\top . Therefore

$$Wp + b \approx (USV^\top)p + b = U(SV^\top p) + b. \quad (16)$$

Instead of having one fully connected layer, now we have 2 but with smaller weight matrices. The first is $SV^\top \in \mathbb{R}^{r \times m}$ and the second is $U \in \mathbb{R}^{n \times r}$. The number of parameters drops from $n \times m$ to $r(n+m)$.

We consider the probabilistic algorithm *variational bayesian matrix factorization* [39] to estimate an optimal rank r of the matrix $W_{m \times n}$. The global solution of VBMF is a reweighted SVD of the observed matrix for use on its approximation.

Finally, we describe a network factorization of a neural implicit function $f_\theta(p) = W_d \circ f_{d-1} \circ \dots \circ f_0(p) + b_d$ with $d-2$ hidden layers $f_i(p) = \varphi(W_i p + b_i)$. As the domain of f_0 is \mathbb{R}^3 and the codomain of W_d is \mathbb{R} , we propose to optimize only the hidden layers of f_θ . For this, we compute the randomized SVD of each hidden weight matrix W_i . The above approach automatically sets the appropriate rank r_i to each weight matrices W_i and Algorithm 1 approximates W_i by a randomized SVD $U_i S_i V_i^\top$. Therefore, we approximate each layer $\varphi(W_i p + b_i)$ of f_θ by $\varphi(U_i(S_i V_i^\top p) + b_i)$ as in Equation (16). This results in a *compact* neural implicit function $f_{\tilde{\theta}}$ with an optimized set of parameters $\tilde{\theta}$. We use this compact network to render images of the underlying implicit neural surface in real-time using a GPU implementation of the sphere tracing algorithm.

4.5 Visualization

To visualize the level sets of a neural implicit function f_θ , we use the *sphere tracing algorithm* [21, 22]. We are assuming $|\nabla f_\theta| \approx 1$. As this algorithm requires several inferences of f_θ along each view ray, we use the above network optimization to obtain a fast inference.

Sphere tracing is appropriate to render level sets of signed distance functions. It operates as follows. Let p_0 and v be the ray origin and ray direction. The intersection between the ray $p_0 + tv$ and the zero-level set $f_\theta^{-1}(0)$ of f_θ is approximated by iterating $p_{n+1} = p_n + v f_\theta(p_n)$. Figure 3 illustrates the algorithm. Therefore, to optimize the computation of the sequence of points p_n , we have to minimize the time spent during each inference $f_\theta(p_n)$.

[49, 31] proposed a network architecture that admits spatial hierarchies decomposition in terms of small neural networks. Although this is the state-of-the-art in terms of neural implicit rendering performance, it comes with essential changes to training and workflow.

When using a single network to represent the surface global geometry, it is already possible to make neural implicit inferences on rendering. [13] implemented sphere tracing in CUDA using NVIDIA

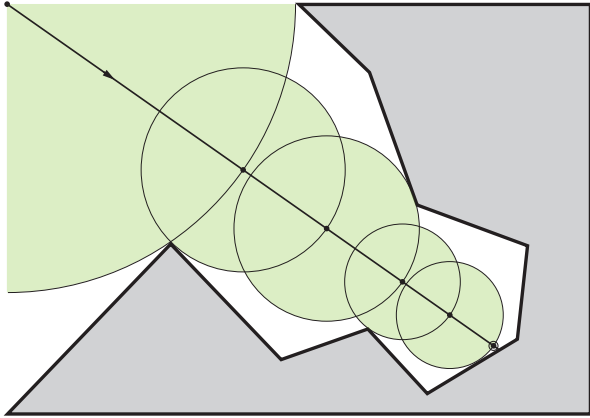


Figure 3: Sphere tracing algorithm.

CUTLASS, a linear algebra library used for efficient matrix multiplication. However, it considers simple networks that seem to lack the capacity to represent the surface’s geometric details.

We use a general network architecture capable of representing surfaces with fine geometry. Then, for a network trained to represent a specific surface, we can optimize its number of parameters using the SVD optimization presented in Section 4.4, without increasing inference timings. Using SVD allows us to select the most important singular values of each weight matrix of the network. The resulting network is a trade-off between compactness and representation capacity, which preserves execution performance.

Inspired by the work of [13], we evaluate the resulting optimized neural implicit function, during the sphere tracing, using an implementation in CUDA and NVIDIA CUTLASS. As a result, we obtain real-time rendering of the neural implicit surfaces.

For shading purposes, the gradient of the level set represents the normal vectors. The gradient of the neural implicit function can be computed using the formula in Section 4.1.1. Associated experiments are presented in Section 5.4.

5 Experiments

Let S be a compact surface inside the cube $\mathcal{Q} = [1, -1]^3$ in \mathbb{R}^3 . In Section 3.1, we saw that there exists a function $f : \mathbb{R}^3 \rightarrow \mathbb{R}$ for which its zero-level set $f^{-1}(0)$ coincides with S , i.e. $f^{-1}(0) = S$. Furthermore, the gradient of f restricted to $f^{-1}(0)$ corresponds to the normals of S . Section 4 presented solutions for the tasks of finding a neural implicit function f_θ that approximates f , optimizing its parameters θ , and visualizing the resulting neural implicit surface. Here, we present the experiments.

Let $T = (V, E, F)$ be a triangulation of S , where $V = \{p_i\}_{i=1}^n \subset S$ are n vertices, E are the edges, and F are the faces. In this section, we consider the triangle mesh T being the Armadillo model since its curvatures are well-distributed. This mesh contains $n = 172974$ vertices. To reconstruct the Armadillo as a neural implicit surface, we use a neural implicit function f_θ with three hidden layers $f_i : \mathbb{R}^{256} \rightarrow \mathbb{R}^{256}$ that use the sine as activation function. See Section 4.1 for the definitions.

We train the parameters θ of f_θ using the loss functional \mathcal{L} discussed in Section 4.2. To find an approximation of a minimum of \mathcal{L} we use the *minibatch gradient descent* [47]:

$$\theta_{k+1} = \theta_k - s_k \nabla_\theta \mathcal{L}(\theta_k), \quad (17)$$

where $\nabla_\theta \mathcal{L}(\theta_k)$ is evaluated on minibatches of size $2m$, with m on-surface points sampled in the dataset $\{p_i\}_{i=1}^n$ and m off-surface points uniformly sampled in the cube \mathcal{Q} . After $\lceil \frac{n}{m} \rceil$ iterations using Equation (17), we have one *epoch* of training, which is equivalent to passing through the whole on-surface dataset once. To compute the *learning rate* s_k we use the ADAM algorithm [25]. We follow the definitions in [48] to compute the first set of parameters θ_0 .

The proposed model can represent geometric details with geometric precision. For example, Figure 4 presents a comparison between the original Armadillo model (right) and its reconstructed neural implicit surface (left) after 1000 epochs of training.

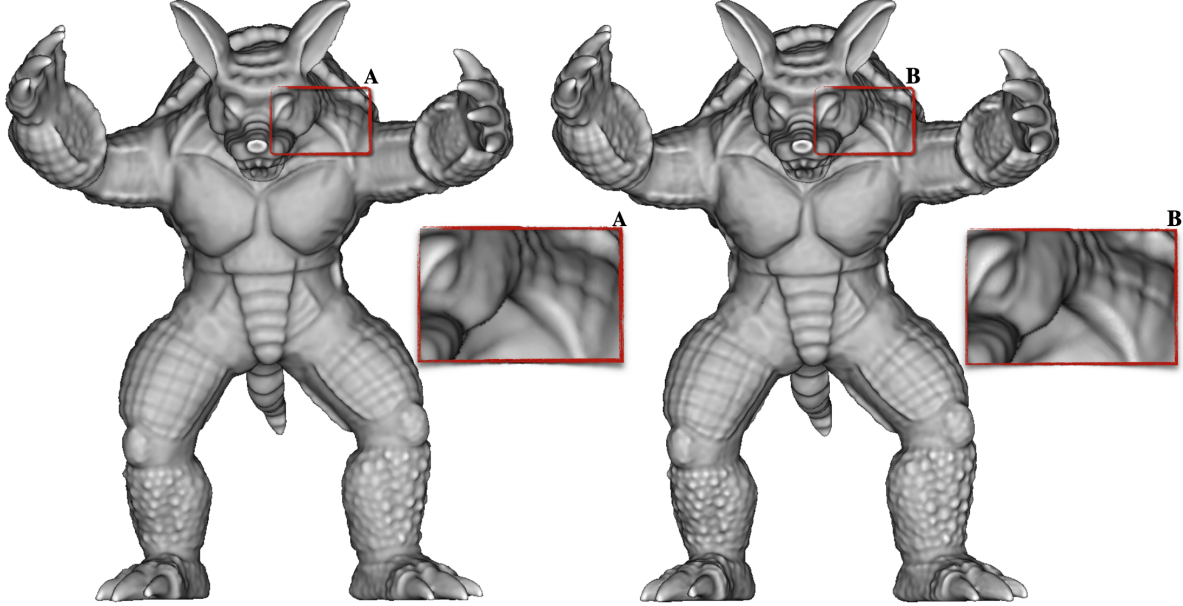


Figure 4: Comparison between the ground truth Armadillo model (right) and its reconstructed neural implicit surface (left) after 1000 epochs of training.

Next, we use the discrete differential geometry of the triangle mesh T to improve the training of the neural implicit function f_θ . We use curvature constraints in the loss function \mathcal{L} and improve the sampling of minibatches in order to prioritize the on-surface points with more geometrical information.

5.1 Loss functional

As we saw in Section 4.2, we can improve the signed distance loss functional $\mathcal{L} = \mathcal{L}_{\text{Eikonal}} + \mathcal{L}_{\text{Dirichlet}} + \mathcal{L}_{\text{Neumann}}$ defined in Equation (4) by adding curvature terms. Here, we consider the alignment between the direction of maximum curvature $(e_1)_\theta$ of the neural implicit surface $f_\theta^{-1}(0)$ and the (discrete) direction of maximum curvature e_1 of the triangle mesh T .

$$\mathcal{L}_{\text{Dir}}(\theta) = \int_E 1 - \langle e_1, (e_1)_\theta \rangle dS \quad (18)$$

Due to possible numerical computation errors, we are restricting this integral term to the region $E \subset S$ where $|\kappa_1 - \kappa_2|$ is high. Remember that regions with $|\kappa_1 - \kappa_2|$ small have points close to *umbilical* points, where the principal directions can not be defined.

Figure 5 compares the training of f_θ using the loss function \mathcal{L} (line 1) with the improved loss function $\mathcal{L} + \mathcal{L}_{\text{Dir}}$ (line 2).

Asking for the alignment between the principal directions during training adds a certain redundancy since we are already asking for the alignment between the normals. Remember that the principal directions are extremes of the differential dN of the normal field N . However, as we can see in Figure 5 it reinforces the learning.

Although it is not a quantitative result, as it does not greatly improve the learning of geometric details, it is a qualitative result. It opens the door for other important applications that depend on adding curvature terms in the loss functional. In particular, it could be used in neural implicit modeling. For example, we could choose certain regions of a neural surface and ask for an enhancement of its geometrical features. Another application could be deforming specific regions of a neural surface using a loss functional that fixes their neighborhood. It is somehow related to *thin plate splines*.

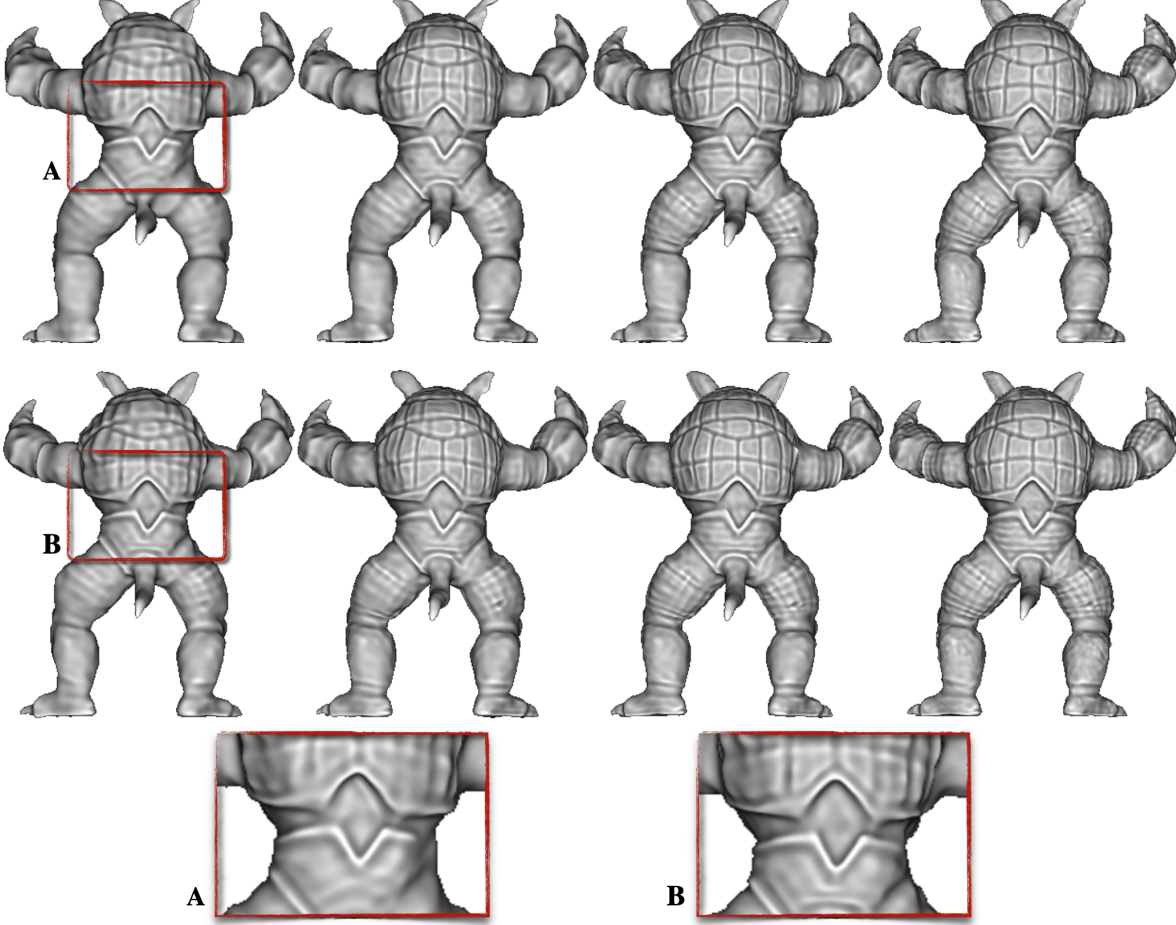


Figure 5: Neural implicit surfaces trained to approximate the Armadillo model. The columns indicate the neural implicit surfaces after 100, 200, 300, and 500 epochs of training. Line 1 shows the results using the signed distance functional. Line 2 presents the results considering the alignment between the principal directions in the loss functional.

5.2 Sampling

This section presents experiments using the sampling strategy discussed in Section 4.3. This proposes selecting minibatches of on-surface points based on the discrete curvatures of the triangle mesh T . It has two important consequences. First, it prioritizes points with important geometric features, those with higher absolute curvatures, during the training implying a fast convergence while preserving quality. Second, this analysis allows finding data redundancy (regions with similar geometry), since points with lower curvature are (in general) more abundant, therefore if we reduce the number of these points during sampling, we train faster.

During the training of the neural network f_θ , it is common to sample minibatches uniformly. Here, we use the curvatures of the triangle mesh T to prioritize the important features. For this, as we discussed in Section 4.3, we split the vertices $\{p_i\}_{i=1}^n$ of T in three sets V_1 , V_2 , and V_3 , with *low*, *medium*, and *high* feature points. We consider the *feature* function being the sum of the absolute of the principal curvatures $\kappa(p_i) = |\kappa_1(p_i)| + |\kappa_2(p_i)|$. Then, choosing $n = n_1 + n_2 + n_3$, with $n_i > 0$ integer, and sorting $\{p_i\}$ using κ , we define the sets $V_1 = \{p_i | i \leq n_1\}$, $V_2 = \{p_i | i > n_1 \text{ and } i \leq n_2\}$, and $V_3 = \{p_i | i > n_2\}$. Observe that $V = V_1 \sqcup V_2 \sqcup V_3$.

We sample minibatches of size $m = p_1m + p_2m + p_3m$, with p_im points on the feature set V_i . In the experiments along this section, we consider $m = 10000$. If this sampling is uniform, we would have $p_i = \frac{n_i}{n}$. Thus, to prioritize points with more geometrical feature, which are those in V_2 and V_3 , we have to reduce p_1 and increase p_2 and p_3 . In other words, we must sample more points with higher feature κ . Figure 6 presents a comparison between the uniform sampling (first line) and the adaptive

sampling (line 2) that consider $p_i = 2^{\frac{n_i}{n}}$ for $i = 2, 3$, i.e. it duplicates the proportion of points with medium and high features. Clearly, these new proportions depend on n_i . In this experiment, we use $n_1 = \frac{n}{2}$, $n_2 = \frac{3n}{10}$, and $n_3 = \frac{n}{10}$, thus V_1 contains half of V . This sampling strategy improved the rate convergence significantly.

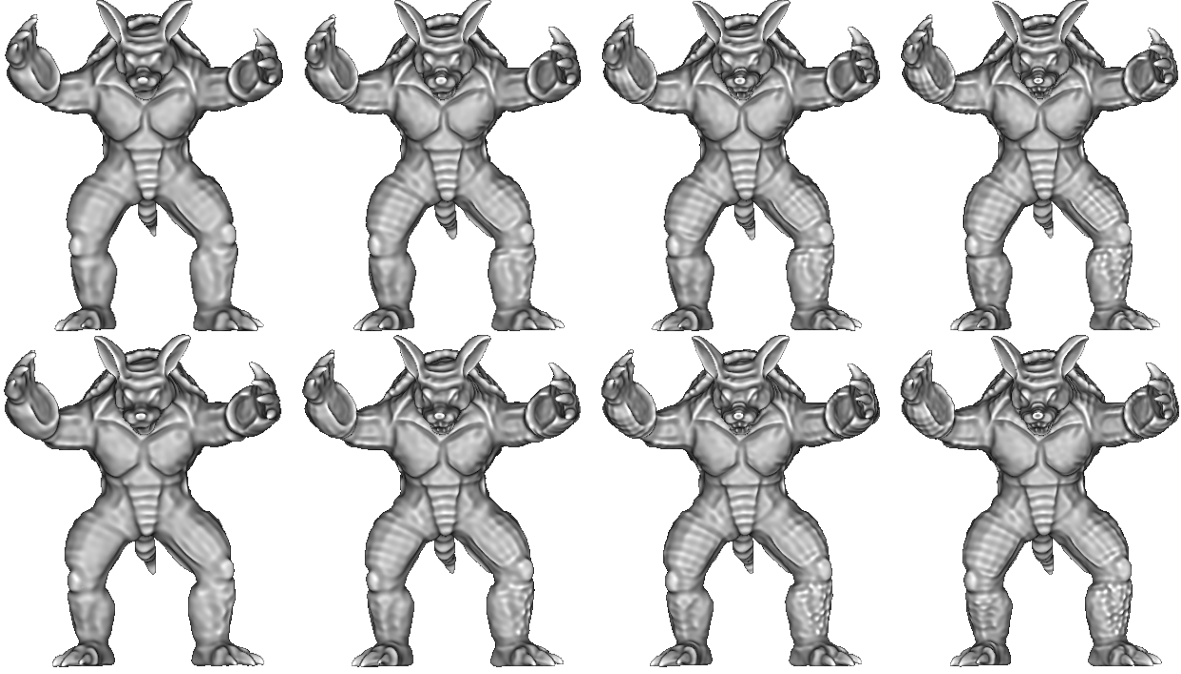


Figure 6: Neural implicit surfaces approximating the Armadillo model. The columns indicate the zero-level sets of the neural implicit functions after 29, 52, 76, and 100 epochs of training. Line 1 shows the results using minibatches sampled uniformly in V . Line 2 presents the results using the adapted sampling of minibatches with 10% / 70% / 20% of points with low/medium/high features.

Removing points in V_1 is equivalent to prioritizing non planar points since the feature function is $\kappa = |\kappa_1| + |\kappa_2|$. The sets V_2 and V_3 are contained in regions with higher (in absolute) principal curvatures. The partition $V = V_1 \sqcup V_2 \sqcup V_3$ resembles the decomposition of the graph of an image in *planar*, *edge*, and *corner* regions, the *Harris corner detector* [20]. Here, $V_2 \cup V_3$ coincides with the union of the edge and corner regions.

Using the absolute of the Gaussian or the mean curvature as the feature function has also improved the training. In the case of the mean curvature, the low feature set V_1 are those regions where the surface is close to a *minimal* surface. These surfaces are defined by having zero mean curvature which is equivalent to locally minimizing the area.

Returning to minibatch sampling. In the last experiment, we were sampling more points with medium and high features in $V_2 \cup V_3$ than points with low features in V_1 . Thus the training visits $V_2 \cup V_3$ more than once per epoch. Therefore, we propose to reduce the number of points sampled per epoch, prioritizing the most important ones. For this, we reduce the size of the minibatch in order to sample each point of $V_2 \cup V_3$ once per epoch.

Figure 7 provides a comparison between the two training strategies. The first line coincides with the experiment presented in the second line of Figure 6. It uses minibatches of size m , and $\lceil \frac{n}{m} \rceil$ iterations of the gradient descent per epoch. In the second line, we sample minibatches of size $\frac{m}{2}$ and use $\lceil \frac{n}{m} \rceil$ iterations of the gradient descent. Then the second line visits half of the dataset in each epoch. We are using the same minibatch proportions p_i and feature sets V_i , as in the previous experiment.

As we can see in Figure 7, going through all the points with medium and higher features once per epoch, while reducing the number of points with low features, resulted in faster training with better quality results. In other words, sampling less points, using the curvatures, results in better quality.

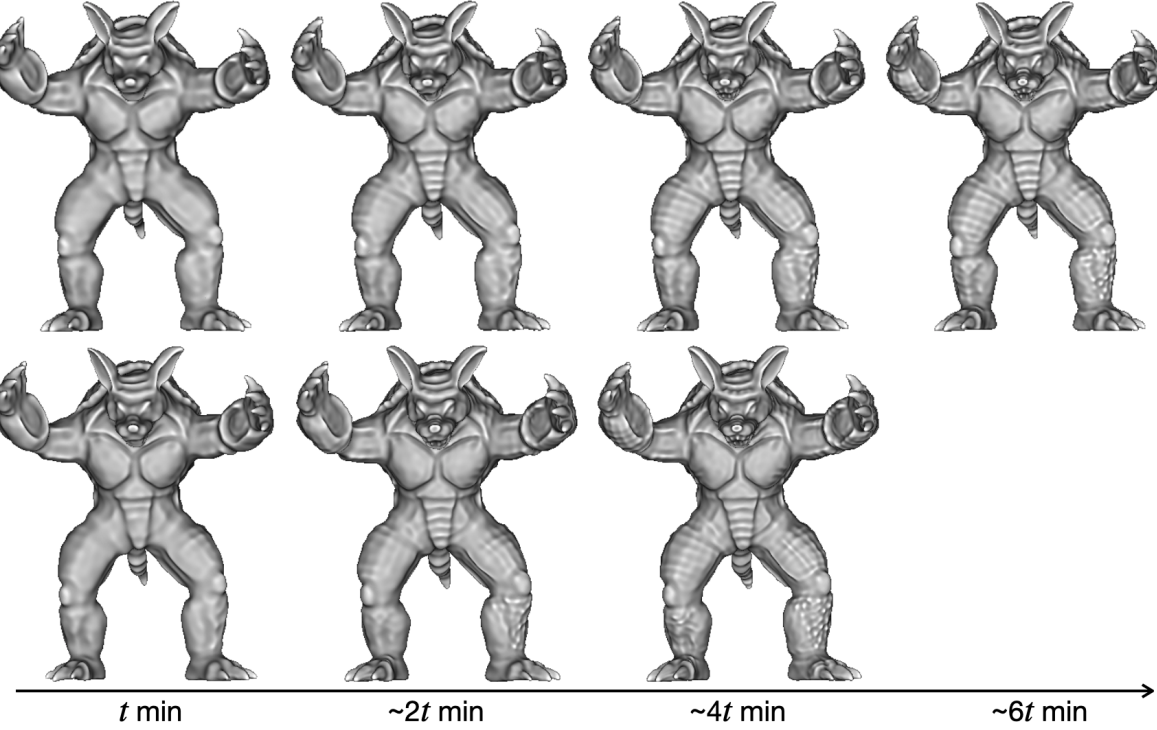


Figure 7: The columns indicate the zero-level sets of the neural implicit functions after t , $2t$, $4t$, and $6t$ minutes of training. Line 1 shows the results using the n points of the dataset per epoch and minibatches of size m containing 20% /60%/20% of points with low/medium/high features. The results in line 2 use $\frac{n}{2}$ points per epoch and minibatches of $\frac{m}{2}$ points with 20% /60%/20% of low/medium/high features. Both experiments use $\lceil \frac{n}{m} \rceil$ steps per epoch.

To keep reducing the size of the minibatches such that we visit important points once per epoch, we have to consider smaller medium and high feature sets. That is, to visit $V_2 \cup V_3$ once per epoch it is necessary to update the sizes n_i of the feature sets V_i . For this, we present three experiments that use $n_1 = \frac{6n}{10}, \frac{75n}{100}, \frac{85n}{100}$, $n_2 = \frac{3n}{10}, \frac{2n}{10}, \frac{n}{10}$, and $n_3 = \frac{n}{10}, \frac{5n}{100}, \frac{5n}{100}$, respectively. Then we can consider minibatches of size $\frac{m}{2}, \frac{3m}{10},$ and $\frac{m}{10}$, i.e. 50%, 30% and 10% of the original minibatch of size m . Figure 8 shows the results of the three experiments. They are all using $\lceil \frac{n}{m} \rceil$ iterations per epoch, therefore, we are visiting $\frac{n}{2}, \frac{3n}{10},$ and $\frac{n}{10}$ points of the dataset on each epoch, respectively. Thus, as we reduce the minibatches sizes we remove points from $V_2 \cup V_3$, which implies that we are going to learn fewer intermediate features. This can be visualized in the figure. Observe that points with higher features are learned faster than points with lower features.

Finding the optimal parameters of the proposed curvature-based sampling can be a hard task for a general triangle mesh. The experiments above show empirically that visiting the "important" points once per epoch implies good geometrical results. One direction to define these important points of a triangle mesh is using the concept of (discrete) *ridge* and *ravine* curves [42]. These are extremes of the principal curvatures along the principal directions [4]. Thus, these salient curves are powerful shape descriptors since they indicate where the surface bends sharply. During sampling, prioritizing points on these curves and on their neighborhood could help us to optimize the number of points used on each epoch of training.

In this section, we discussed the sampling of on-surface points. The sampling of off-surface points is still uniform in the cube \mathcal{Q} . An interesting path for future work is the optimization of this sampling using the *tubular neighborhood* of the triangle mesh T . See Section 6.1 for more comments.

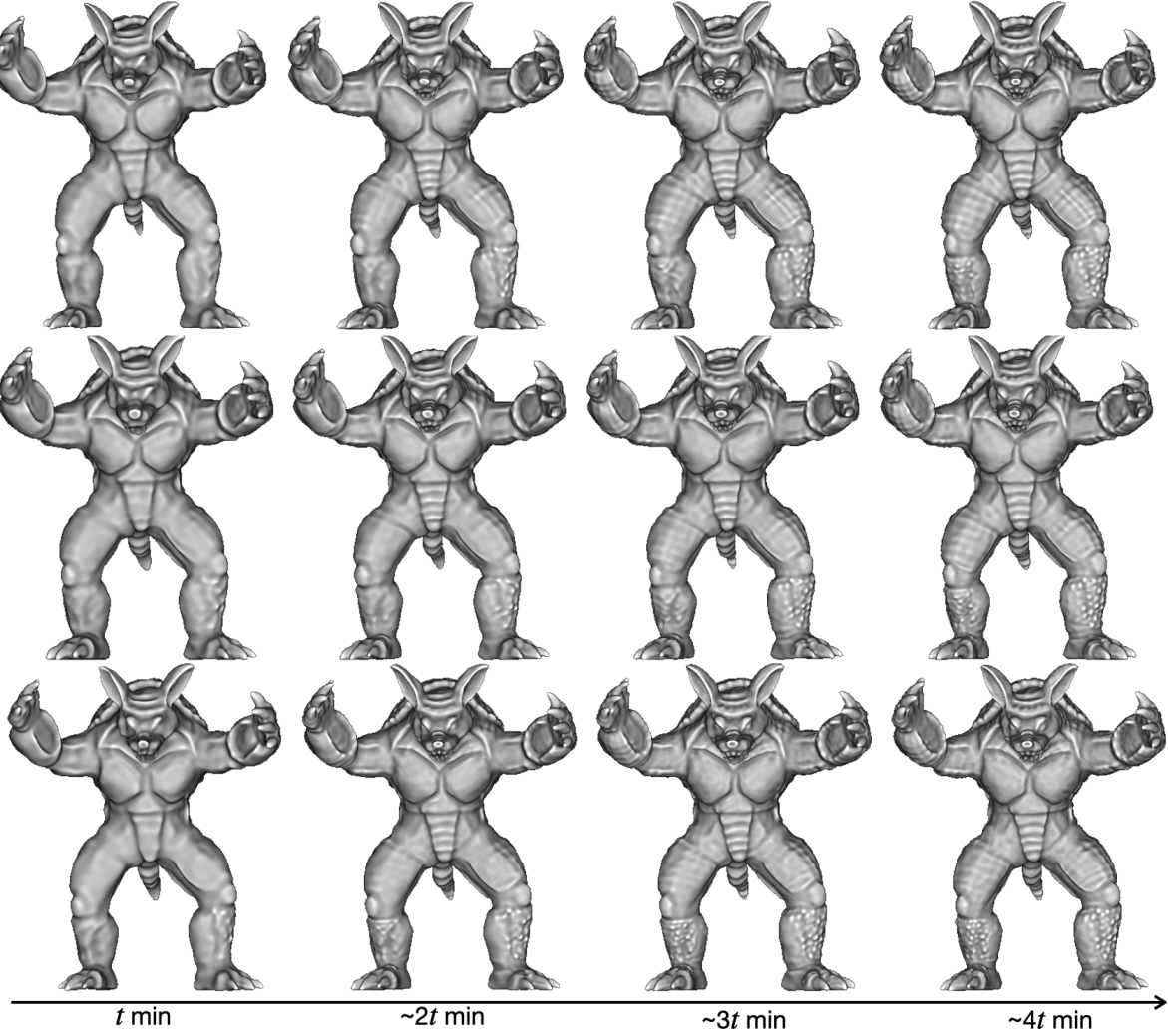


Figure 8: The columns present the zero-level sets of the model after t , $2t$, $3t$, and $4t$ minutes of training. The results in line 1 use $\frac{n}{2}$ points per epoch and minibatches of $\frac{m}{2}$ points with 20% /60%/20% of low/medium/high features. Line 2 shows the results using $\frac{3n}{10}$ points per epoch and minibatches of $\frac{3m}{10}$ points with 17% /67%/17% of low/medium/high features. The results in line 3 use $\frac{n}{10}$ points per epoch and minibatches of $\frac{m}{10}$ points with 10% /70%/20% of low/medium/high features. The experiments use $\lceil \frac{n}{m} \rceil$ steps per epoch.

5.3 Network optimization

The next experiment further optimizes a trained neural implicit function using the ideas of Section 4.4. Let f_θ be a trained neural implicit function consisting of three hidden layers $f_i(p_i) = \varphi(W_i p_i + b_i)$, where $W_i \in \mathbb{R}^{256 \times 256}$ are the weight matrices and $b_i \in \mathbb{R}^{256}$ are the biases. To optimize the parameters θ , we use the singular value decomposition of each weight matrix W_i . More precisely, we truncate it, keeping only its first r most important singular values:

$$W_i \approx (U_i S_i V_i^\top) = U_i (S_i V_i^\top). \quad (19)$$

Where $U_i, V_i^\top \in \mathbb{R}^{256 \times r}$ and $S_i \in \mathbb{R}^{r \times r}$. Then, instead of the layer $W_i \in \mathbb{R}^{256 \times 256}$, we have the layers $S V^\top$ and U with smaller weight matrices. Thus, the number of parameters of each hidden layer drops from 256^2 to $2 \cdot r \cdot 256$. The first layer $f_0 : \mathbb{R}^3 \rightarrow \mathbb{R}^{256}$ and the last $f_3 : \mathbb{R}^{256} \rightarrow \mathbb{R}$ of f_θ are maintained. We denote the resulting decomposed neural network by f_{θ_r} .

Figure 9 presents the experiments of decomposing the three hidden layers $f_i : \mathbb{R}^{256} \rightarrow \mathbb{R}^{256}$ of the neural implicit function f_θ , trained during 1000 epochs to represent the Armadillo model. We consider three decompositions of f_θ using $r = 32, 16, 8$ singular values, respectively.



Figure 9: Decomposed neural surfaces trained to represent the Armadillo model. From left to right, we have the original neural implicit surface $f_\theta^{-1}(0)$, and its approximations $f_{\theta_{32}}^{-1}(0)$, $f_{\theta_{16}}^{-1}(0)$, and $f_{\theta_8}^{-1}(0)$.

Observe that θ_{32} has 25.77% of the weights of θ , however, $f_{\theta_{32}}$ still represents fine details of the Armadillo surface. Using 16 singular values, the number of weights in θ_{16} drops to 13.40% of the size of θ . Even so, the surface is represented with a reasonable detail. With only 7.22% of the weights of θ , f_{θ_8} cannot represent the geometry details of the Armadillo, only its global shape.

It is important to note that each decomposed neural implicit function f_{θ_r} was retrained. Therefore, we cannot (yet) use f_{θ_r} to represent f_θ hierarchically. However, finding an integer r such that f_{θ_r} represents f_θ is very helpful since we can reduce the number of parameters significantly, as we saw in the experiment above. Next we use this decomposition to speed up the sphere tracing of the underlying neural implicit surface $f_\theta^{-1}(0)$.

5.4 Visualization using sphere tracing

In this section, we use the sphere tracing algorithm (Sec. 4.5) to render images of a neural implicit surface $f_\theta^{-1}(0)$. The corresponding network f_θ was trained to approximate the signed distance function of the Armadillo model.

An important advantage of using neural implicit functions to represent surfaces is that we can compute their differentiable objects analytically. For example, Figure 10 shows two shadings of the neural surface $f_\theta^{-1}(0)$. On the left, the image was rendered using the traditional *Phong* shading, and on the right, we use a *transfer function* to visualize the mean curvature of the neural surface. Both normal vectors and mean curvature were calculated analytically through their formulas $\frac{\nabla f_\theta}{|\nabla f_\theta|}$ and $\text{div } \frac{\nabla f_\theta}{|\nabla f_\theta|}$ using `torch.autograd`.

While neural surface visualizations are quite accurate, when considering real-time applications, we run into performance issues. In other words, it is unpractical to use these methods in real-time CPU applications due to their computational complexity. For example, each inference in the non-decomposed network f_θ takes 1.87 seconds (on average) using Pytorch in the CPU. To speed up the inference, we use the decomposed network $f_{\theta_{27}}$, which considers the optimal singular values of the SVD (Sec. 5.3), as a result we obtain the inference in 1.35 seconds (on average).

To provide a real time visualization of the neural implicit surface $f_\theta^{-1}(0)$, we propose a sphere tracing implementation in GPU using CUDA and NVIDIA CUTLASS. Figure 11 presents a 512×512 image of the neural surface $f_\theta^{-1}(0)$ with a frame rate of 17 fps. No bounding boxes or acceleration structures are used, so all pixels are evaluated. The sphere tracing iterates 25 times, and we consider that a ray reaches the surface if the distance falls below a threshold of 0.05 after all iterations. We compute the normal vectors of the neural surface $f_\theta^{-1}(0)$ at the hit points using Equation (7). Again, lighting is done using traditional Phong model. See [12], for more details on the rendering of neural implicits.

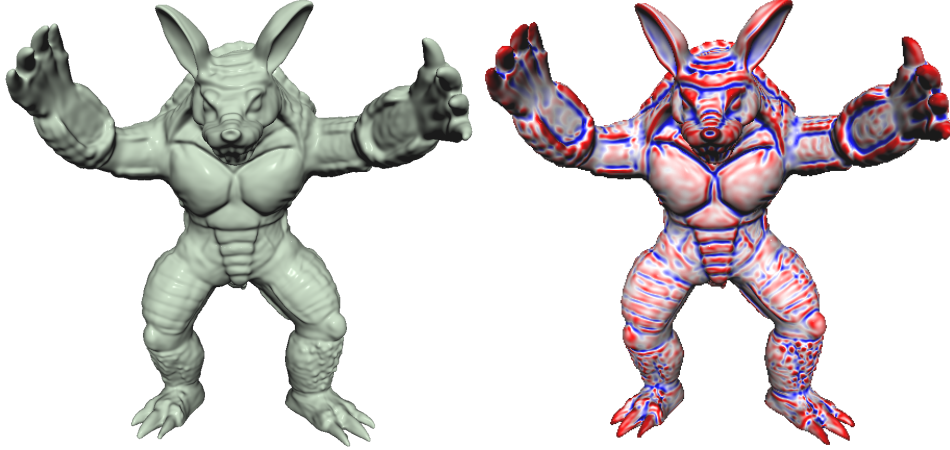


Figure 10: Sphere tracing of the neural surface $f_\theta^{-1}(0)$, trained to represent the Armadillo model. On the Left, the shading uses the normal vectors computed analytically using `torch.autograd`. On the right, we used a *transfer function* to visualize the mean curvature of the neural surface. This function relates points with high/medium/low curvatures to the red/white/blue colors.

6 Conclusions and future works

We introduced a neural network framework that exploits the differentiable properties of neural implicit functions and the discrete geometry of triangle meshes to represent them as neural implicit surfaces. The proposed loss functional can consider terms with high order derivatives, such as the alignment between the principal directions of curvatures. As a result, we obtained reinforcement in the training, gaining more geometric details. This motivates future applications, for example, implicit surface modeling, since many modeling applications require the minimization of an energy functional that includes curvature terms, such as the Willmore energy.

We also present a sampling strategy based on the discrete curvatures of the triangle mesh. This allowed us to access points with more geometric information during the sampling of minibatches. As a result, this optimization trains faster and has better geometric accuracy, since we were able to reduce the number of points in each minibatch by prioritizing the important points.

To visualize the resulting neural implicit surface in real-time, we presented an implementation of the sphere tracing in GPU. As such an algorithm requires many inferences along each view ray, we had to optimize the number of operations on each inference. For this, we proposed an optimization of the network based on the singular value decomposition of the network’s hidden weight matrices.

In this article, we emphasized the sampling of on-surface points during the training. Future work includes a sampling of off-surface points. Using the *tubular neighborhood* of the triangle mesh can be a direction to improve the sampling of off-surface points.

6.1 Tubular neighborhood

The tubular neighborhood of a compact surface S is the disjoint union $\cup_{p \in S} I_p$ of intervals $I_p = \{q \in \mathbb{R}^3 | q = p + tN\}$, where N is the normal field of S and t belong to an interval $(-l(p), l(p))$. The *local feature size* $l(p)$ can be computed using the *medial axis* $\text{Med}(S)$ of S , which is the set of points having at least two closest points in S . For each $p \in S$, $l(p)$ is the distance of p to $\text{Med}(S)$.

The medial axis of the surface S is contained in the set of critical points of its signed distance function, therefore, its should not be used in the term $\mathcal{L}_{\text{Eikonal}}$ of the loss function given in Equation (4). Moreover, exploring the properties of the medial axis and local feature size function of S could help in the sampling of off-surface points since these are important tools in surface reconstruction [33, 3].

In the tubular neighborhood $\cup I_p$ of S we can easily compute the signed distance of S and its gradient. Indeed, for a point $q \in I_p$ note that by its definition $q = p + tN$, then, its signed distance to S is t and the gradient is N . During training of a neural implicit function, minibatches of off-surface points near to S can be sampled by selecting points directly on the lines $\{I_p\}$.



Figure 11: Real time sphere tracing in the GPU of a neural surface trained to represent the Armadillo.

We have also the notion of curvature in the tubular neighborhood of S . More precisely, consider a family of *parallel surfaces* to S defined by $S_t = \{q \in \mathbb{R}^3 | q = p + tN, N \text{ is the normal at } p \in S\}$ with $t \in I_p$. Gaussian and mean curvatures at a point $q = p + tN$ can be computed [15, Page 215].

$$K' = \frac{K}{1 - 2tH + t^2K} \text{ and } H' = \frac{H - tK}{1 - 2tH + t^2K}. \quad (20)$$

Where K and H are the Gaussian and mean curvatures of S at p . Therefore, we could also develop a curvature biased sampling of off-surface points.

6.2 Comments about the divergence theorem

The *divergence theorem* translates the constraint $\int 1 - \langle \nabla f_\theta, N \rangle dS$ on the surface S to its interior region, which we denote by \mathcal{V} . More precisely, using the divergence theorem we get

$$\int_S \langle \nabla f_\theta, N \rangle dS = \int_{\mathcal{V}} \Delta f_\theta(p) dp,$$

where $S = \partial\mathcal{V}$, N is the normal field of S , and Δf_θ is *Laplacian* of f_θ which is the divergent of the gradient of f_θ . Therefore, we obtain

$$\int_S (1 - \langle \nabla f_\theta, N \rangle) dS = |S| - \int_{\mathcal{V}} \Delta f_\theta(p) dp, \quad (21)$$

where $|S|$ is the area of S .

The advantage of the above observation is that the normal field is not used on the right side of Equation (21), therefore, during training, the point cloud $\{p_i, N_i\}$ does not need to consider the normals $\{N_i\}$, only the area of the sampled surface must be considered. To select points in \mathcal{V} , just consider the points with the distance (to the S surface) less than or equal to zero.

References

- [1] Pierre Alliez, David Cohen-Steiner, Olivier Devillers, Bruno Lévy, and Mathieu Desbrun. Anisotropic polygonal remeshing. In *ACM SIGGRAPH 2003 Papers*, pages 485–493. 2003.
- [2] Nina Amenta, Sunghee Choi, Tamal K Dey, and Naveen Leekha. A simple algorithm for homeomorphic surface reconstruction. In *Proceedings of the sixteenth annual symposium on Computational geometry*, pages 213–222, 2000.
- [3] Nina Amenta, Sunghee Choi, and Ravi Krishna Kolluri. The power crust. In *Proceedings of the sixth ACM symposium on Solid modeling and applications*, pages 249–266, 2001.
- [4] Alexander G Belyaev, Alexander A Pasko, and Tosiyasu L Kunii. Ridges and ravines on implicit surfaces. In *Proceedings. Computer Graphics International (Cat. No. 98EX149)*, pages 530–535. IEEE, 1998.
- [5] Nuri Benbarka, Timon Höfer, Andreas Zell, et al. Seeing implicit neural representations as fourier series. *arXiv preprint arXiv:2109.00249*, 2021.
- [6] Jonathan C Carr, Richard K Beatson, Jon B Cherrie, Tim J Mitchell, W Richard Fright, Bruce C McCallum, and Tim R Evans. Reconstruction and representation of 3d objects with radial basis functions. In *Proceedings of the 28th annual conference on Computer graphics and interactive techniques*, pages 67–76, 2001.
- [7] Zhiqin Chen, Andrea Tagliasacchi, and Hao Zhang. Bsp-net: Generating compact meshes via binary space partitioning. *Proceedings of IEEE Conference on Computer Vision and Pattern Recognition (CVPR)*, 2020.
- [8] Zhiqin Chen and Hao Zhang. Learning implicit fields for generative shape modeling, 2019.
- [9] David Cohen-Steiner and Jean-Marie Morvan. Restricted delaunay triangulations and normal cycle. In *Proceedings of the nineteenth annual symposium on Computational geometry*, pages 312–321, 2003.
- [10] Keenan Crane. *An Excursion Through Discrete Differential Geometry: AMS Short Course, Discrete Differential Geometry, January 8-9, 2018, San Diego, California*. American Mathematical Soc., 2020.
- [11] George Cybenko. Approximation by superpositions of a sigmoidal function. *Mathematics of control, signals and systems*, 2(4):303–314, 1989.
- [12] Vinícius da Silva, Tiago Novello, Guilherme Schardong, Luiz Schirmer, Hélio Lopes, and Luiz Velho. Mip-plicits: Level of detail factorization of neural implicits sphere tracing. *arXiv preprint*, 2022.
- [13] Thomas Davies, Derek Nowrouzezahrai, and Alec Jacobson. On the effectiveness of weight-encoded neural implicit 3d shapes, 2021.
- [14] Boyang Deng, Kyle Genova, Soroosh Yazdani, Sofien Bouaziz, Geoffrey Hinton, and Andrea Tagliasacchi. Cvxnet: Learnable convex decomposition. June 2020.
- [15] Manfredo P Do Carmo. *Differential geometry of curves and surfaces: revised and updated second edition*. Courier Dover Publications, 2016.
- [16] Kyle Genova, Forrester Cole, Avneesh Sud, Aaron Sarna, and Thomas A. Funkhouser. Deep structured implicit functions. *CoRR*, abs/1912.06126, 2019.
- [17] Ron Goldman. Curvature formulas for implicit curves and surfaces. *Computer Aided Geometric Design*, 22(7):632–658, 2005.
- [18] Meenakshisundaram Gopi, Shankar Krishnan, and Cláudio T Silva. Surface reconstruction based on lower dimensional localized delaunay triangulation. In *Computer Graphics Forum*, volume 19, pages 467–478. Wiley Online Library, 2000.

- [19] Amos Gropp, Lior Yariv, Niv Haim, Matan Atzmon, and Yaron Lipman. Implicit geometric regularization for learning shapes. *arXiv preprint arXiv:2002.10099*, 2020.
- [20] Christopher G Harris, Mike Stephens, et al. A combined corner and edge detector. In *Alvey vision conference*, volume 15, pages 10–5244. Citeseer, 1988.
- [21] John C Hart. Sphere tracing: A geometric method for the antialiased ray tracing of implicit surfaces. *The Visual Computer*, 12(10):527–545, 1996.
- [22] John C Hart, Daniel J Sandin, and Louis H Kauffman. Ray tracing deterministic 3-D fractals. In *Proceedings of the 16th Annual Conference on Computer Graphics and Interactive Techniques*, pages 289–296, 1989.
- [23] Klaus Hildebrandt, Konrad Polthier, and Max Wardetzky. Smooth feature lines on surface meshes. In *Symposium on geometry processing*, pages 85–90, 2005.
- [24] Gordon Kindlmann, Ross Whitaker, Tolga Tasdizen, and Torsten Moller. Curvature-based transfer functions for direct volume rendering: Methods and applications. In *IEEE Visualization, 2003. VIS 2003.*, pages 513–520. IEEE, 2003.
- [25] Diederik P Kingma and Jimmy Ba. Adam: A method for stochastic optimization. *arXiv preprint arXiv:1412.6980*, 2014.
- [26] Carsten Lange and Konrad Polthier. Anisotropic smoothing of point sets. *Computer Aided Geometric Design*, 22(7):680–692, 2005.
- [27] Guillaume Lavoué, Florent Dupont, and Atilla Baskurt. A new cad mesh segmentation method, based on curvature tensor analysis. *Computer-Aided Design*, 37(10):975–987, 2005.
- [28] Thomas Lewiner, Hélio Lopes, Antônio Wilson Vieira, and Geovan Tavares. Efficient implementation of marching cubes’ cases with topological guarantees. *Journal of graphics tools*, 8(2):1–15, 2003.
- [29] Ives Macedo, Joao Paulo Gois, and Luiz Velho. Hermite radial basis functions implicits. In *Computer Graphics Forum*, volume 30, pages 27–42. Wiley Online Library, 2011.
- [30] Martin Marinov and Leif Kobbelt. Direct anisotropic quad-dominant remeshing. In *12th Pacific Conference on Computer Graphics and Applications, 2004. PG 2004. Proceedings.*, pages 207–216. IEEE, 2004.
- [31] Julien NP Martel, David B Lindell, Connor Z Lin, Eric R Chan, Marco Monteiro, and Gordon Wetzstein. Acorn: Adaptive coordinate networks for neural scene representation. *arXiv preprint arXiv:2105.02788*, 2021.
- [32] Per-Gunnar Martinsson, Vladimir Rokhlin, and Mark Tygert. A randomized algorithm for the decomposition of matrices. *Applied and Computational Harmonic Analysis*, 30(1):47–68, 2011.
- [33] Boris Mederos, Nina Amenta, Luiz Velho, and Luiz Henrique De Figueiredo. Surface reconstruction for noisy point clouds. In *Symposium on Geometry Processing*, pages 53–62. Citeseer, 2005.
- [34] Lars M. Mescheder, Michael Oechsle, Michael Niemeyer, Sebastian Nowozin, and Andreas Geiger. Occupancy networks: Learning 3d reconstruction in function space. *CoRR*, abs/1812.03828, 2018.
- [35] Mark Meyer, Mathieu Desbrun, Peter Schröder, and Alan H Barr. Discrete differential-geometry operators for triangulated 2-manifolds. In *Visualization and mathematics III*, pages 35–57. Springer, 2003.
- [36] Mateusz Michalkiewicz. Implicit surface representations as layers in neural networks. In *International Conference on Computer Vision (ICCV)*. IEEE, 2019.
- [37] Ben Mildenhall, Pratul P Srinivasan, Matthew Tancik, Jonathan T Barron, Ravi Ramamoorthi, and Ren Ng. Nerf: Representing scenes as neural radiance fields for view synthesis. In *European conference on computer vision*, pages 405–421. Springer, 2020.

- [38] Niloy J Mitra, Leonidas J Guibas, and Mark Pauly. Partial and approximate symmetry detection for 3d geometry. *ACM Transactions on Graphics (TOG)*, 25(3):560–568, 2006.
- [39] Shinichi Nakajima, Masashi Sugiyama, S Derin Babacan, and Ryota Tomioka. Global analytic solution of fully-observed variational bayesian matrix factorization. *Journal of Machine Learning Research*, 14(Jan):1–37, 2013.
- [40] Tiago Novello, Vinícius da Silva, Guilherme Schardong, Luiz Schirmer, Hélio Lopes, and Luiz Velho. Neural implicit surfaces in higher dimension. *arXiv preprint*, 2022.
- [41] Michael Oechsle, Songyou Peng, and Andreas Geiger. Unisurf: Unifying neural implicit surfaces and radiance fields for multi-view reconstruction. In *International Conference on Computer Vision (ICCV)*, 2021.
- [42] Yutaka Ohtake, Alexander Belyaev, and Hans-Peter Seidel. Ridge-valley lines on meshes via implicit surface fitting. In *ACM SIGGRAPH 2004 Papers*, pages 609–612. 2004.
- [43] Jeong Joon Park, Peter Florence, Julian Straub, Richard Newcombe, and Steven Lovegrove. Deepsdf: Learning continuous signed distance functions for shape representation. In *Proceedings of the IEEE/CVF Conference on Computer Vision and Pattern Recognition*, pages 165–174, 2019.
- [44] Songyou Peng, Michael Niemeyer, Lars M. Mescheder, Marc Pollefeys, and Andreas Geiger. Convolutional occupancy networks. *CoRR*, abs/2003.04618, 2020.
- [45] Ravi Ramamoorthi, Dhruv Mahajan, and Peter Belhumeur. A first-order analysis of lighting, shading, and shadows. *ACM Transactions on Graphics (TOG)*, 26(1):2–es, 2007.
- [46] Shaoqing Ren, Kaiming He, Ross Girshick, and Jian Sun. Faster R-CNN: Towards real-time object detection with region proposal networks. *Advances in neural information processing systems*, 28:91–99, 2015.
- [47] Sebastian Ruder. An overview of gradient descent optimization algorithms. *arXiv preprint arXiv:1609.04747*, 2016.
- [48] Vincent Sitzmann, Julien Martel, Alexander Bergman, David Lindell, and Gordon Wetzstein. Implicit neural representations with periodic activation functions. *Advances in Neural Information Processing Systems*, 33, 2020.
- [49] Towaki Takikawa, Joey Litalien, Kangxue Yin, Karsten Kreis, Charles Loop, Derek Nowrouzezahrai, Alec Jacobson, Morgan McGuire, and Sanja Fidler. Neural geometric level of detail: Real-time rendering with implicit 3d shapes. *arXiv preprint arXiv:2101.10994*, 2021.
- [50] Gabriel Taubin. Estimating the tensor of curvature of a surface from a polyhedral approximation. In *Proceedings of IEEE International Conference on Computer Vision*, pages 902–907. IEEE, 1995.
- [51] Peng Wang, Lingjie Liu, Yuan Liu, Christian Theobalt, Taku Komura, and Wenping Wang. Neus: Learning neural implicit surfaces by volume rendering for multi-view reconstruction. *NeurIPS*, 2021.
- [52] Max Wardetzky, Saurabh Mathur, Felix Kälberer, and Eitan Grinspun. Discrete laplace operators: no free lunch. In *Symposium on Geometry processing*, pages 33–37. Aire-la-Ville, Switzerland, 2007.
- [53] Lior Yariv, Jiatao Gu, Yoni Kasten, and Yaron Lipman. Volume rendering of neural implicit surfaces, 2021.
- [54] Lior Yariv, Yoni Kasten, Dror Moran, Meirav Galun, Matan Atzmon, Ronen Basri, and Yaron Lipman. Multiview neural surface reconstruction by disentangling geometry and appearance. *arXiv preprint arXiv:2003.09852*, 2020.